Quantum Scattering with Energy-Filtered Plane Wave Packets: Visualizing the F + HD "Ridge" Mechanism†

Stuart C. Althorpe*

School of Chemistry, University of Exeter, Stocker Road, Exeter EX4 4QD, United Kingdom

Received: March 24, 2003; In Final Form: May 7, 2003

We develop a very simple, previously neglected, idea for enhancing the power of quantum wave packet calculations to interpret chemical reactions. This is that, once the energy-domain wave function is calculated, an infinite variety of time-dependent wave packets may be recovered from it, simply by multiplying by an energy filter and taking the Fourier transform. Each packet corresponds to a different initial wave packet along the scattering coordinate. We show that, when incorporated into the plane wave packet method [*J. Chem. Phys.* **2002**, *117*, 4623], the filters can isolate features in the differential cross section and generate separate wave packets visualizing the dynamics of each feature. The filters also enable one to focus the wave packets, so as to minimize artifacts caused by spreading. We demonstrate these ideas on the F + HD reaction, by isolating the low energy ridge from the differential cross section and generating a focused plane wave packet that visualizes its dynamics. We find that the ridge is produced by a "Catherine wheel" rotation and decay of the FHD complex through about 180°.

I. Introduction

Wave packet calculations give unique insight into the quantum dynamics of chemical processes, by yielding "movies" which visualize the motion of the atoms. The movies can be used to simulate the time-evolution of a femtochemistry experiment,[1] or they can be used to interpret an energy-domain experiment, by comparing with data obtained over a spread of energies. The latter type of interpretation has been applied to a variety of systems, including molecular photodissociation,[2−5] molecule−surface interactions,[6−8] rate constant predictions,[9] and, the subject of the present paper, quantum reactive scattering.[10−22]

Wave packet methods were introduced into quantum scattering[11−13] because they scale better than time-independent methods, and this advantage led to the first accurate calculations of cross sections for 4-atom reactions.[14,15] However, a growing body of work (e.g., refs. 16−22) has also exploited the ability of wave packets to visualize the dynamics. Such visualization is especially useful for reactions, because it provides a link between the "physics" language of time-independent scattering theory, and the "chemistry" language of "reaction mechanisms". It also makes possible direct comparisons with quasiclassical trajectory (QCT) calculations.[23]

The present paper addresses a largely overlooked aspect of the use of wave packets to visualize quantum reactive scattering. This is that, because one is interpreting an energy-domain experiment, the choice of the initial wave packet is largely arbitrary. The internal states of the reagents, and the overall spread of collision energies, must of course be the same in the initial wave packet as in the experiment. However, the precise form of the collision energy spread, and hence the shape and position of the initial wave packet along the scattering coordinate, are largely undetermined. The only restriction is that the initial wave packet be placed sufficiently far out, that the scattering potential can be neglected.[11−13] Typically, the initial wave packet is chosen to be a Gaussian, and just one initial wave packet is propagated for each initial quantum state of the reagents.

However, there will be occasions when several, or indeed many, initial wave packets should be propagated for each initial quantum state of the reagents. First, it may be necessary to test whether the wave packets contain artifacts dependent upon the form of the initial packet. For example, at low collision energies, spreading of the wave packet will occur, and this might be mistaken for the effects of a trapping mechanism. The true cause of the spreading could be unmasked by varying the initial position of the wave packet. Second, the calculated cross sections or reaction probabilities may contain distinct features as a function of energy, or scattering angle. In such cases, it would be interesting to prepare different wave packets containing different spreads of collision energies, each of which would visualize the dynamics responsible for one of the features. Almost certainly this would require quite a lot of experimentation, with different energy filters being tested, to isolate smoothly the features without introducing artifacts.

Thus, one can imagine many examples where reactions could be interpreted more clearly, and in more detail, by propagating a series of different packets for each initial quantum state of the reagents. Given that this is so, we are surprised that, to date, almost all wave packet calculations of reaction dynamics have been done starting with just one wave packet (per initial quantum state of the reagents). However, if one wave packet can be propagated, then as many different wave packets as desired may be recovered from it. One has simply to generate the time-independent wave function $\Phi(E)$ over a grid of collision energies E, store it on disk, and then transform back using[24]

$$\chi(t) = \int_0^\infty F(E)\Phi(E)\mathrm{e}^{-iEt/\hbar}\,\mathrm{d}E \qquad (1)$$

This equation may be applied as many times as desired, using a series of different energy filters $F(E)$, to generate a series of

† Part of the special issue "Donald J. Kouri Festschrift".

* To whom correspondence should be addressed. E-mail: s.c.althorpe@ex.ac.uk.

10.1021/jp0303671 CCC: $25.00
Published on Web 06/20/2003

wave packets $\chi(t)$. Each packet will describe the time-evolution of a different initial wave packet, whose form along the scattering coordinate is determined by $F(E)$. Almost certainly, this approach was not adopted previously because, for a realistic scattering problem, a lot of disk space is required to store $\Phi(E)$. However, disk space is now very cheap—even a desktop PC may hold several hundred gigabytes. Hence, eq 1 is a simple, practical way to generate a series of $\chi(t)$ corresponding to different initial packets along the scattering coordinate.

In the present paper, we test out the ideas just discussed by applying eq 1 within the plane wave packet (PWP) method, to the F + HD reaction, in the collision energy range $E = 0-0.15$ eV. The PWP method was introduced recently by the author[20-22] as a means of generating wave packets to visualize how the products of a reactive (or inelastic) collision scatter into space. The (energy-domain) differential cross sections are obtained directly from these wave packets, via time-dependent differential cross sections.[20] Hence, the use of eq 1 in the PWP method would permit one to isolate distinct features in the differential cross section and to generate wave packets showing the scattering into space that produces them. The F + HD reaction, in the range, $E = 0-0.15$ eV, is an ideal system to demonstrate these ideas. First, the low collision energies allow one to investigate artifacts caused by spreading of the wave packet. Second, the differential cross sections contain distinct features, caused by separate direct and time-delayed mechanisms.[19,22,25,26] We will pay particular attention to one of the time-delayed mechanisms, which appears as a "ridge" in the differential cross section and was shown recently[19,25,26] to be the first conclusive evidence of Feshbach resonances in reactive scattering.

The paper is organized as follows. Section II provides the theory needed to apply eq 1 within the PWP method. It starts (II.A) with some background to eq 1; summarizes (II.B) the PWP method; explains (II.C) how to implement eq 1 within the PWP method; and discusses (II.D) how to use the filter $F(E)$ to focus the initial plane wave packet. Section III describes the application to F + HD and concentrates on the dynamics of the "ridge" mechanism. Section IV concludes with suggestions of further developments to the simple filtering ideas presented here.

II. Theory

A. Generating Wave Packets using Energy Filters. Before discussing how to use eq 1 in the plane wave packet method, it is useful to revise the derivation of this equation and to point out the conditions under which it can be applied. It is sufficient to consider the simplest case of one-dimensional scattering along a coordinate x.

At time $t = 0$, the initial wave packet $\chi(x|0)$ is placed at a sufficiently large value of x that the scattering potential $V(x)$ can be neglected. The time-dependent wave packet $\chi(x|t)$ describing the scattering is then given by

$$\chi(x|t) = \mathrm{e}^{-iHt/\hbar}\chi(x|0) \tag{2}$$

Let us examine the energy composition of $\chi(x|t)$. There are various (equivalent) ways of doing this; one of the clearest is to use the time-independent wave packet (TIWP) formulation.[27] This defines the TIWP function

$$\xi(x|E) = \frac{1}{2\pi\hbar}\int_0^\infty \chi(x|t)\mathrm{e}^{iEt/\hbar}\,\mathrm{d}t \tag{3}$$

which is the solution of the inhomogeneous Schrödinger equation

$$(E - H)\xi(x|E) = \frac{i}{2\pi}\chi(x|0) \tag{4}$$

It can be shown[27] that, for all values of x on the potential side of $\chi(x|0)$, the TIWP solution $\xi(x|E)$ satisfies

$$\xi(x|E) = F(E)\Phi(x|E) \tag{5}$$

where $\Phi(x|E)$ is the usual scattering solution to the time-independent Schrödinger equation. The energy filter $F(E)$ is given by[27]

$$F(E) = \frac{mA(k)}{\hbar^2 k} \tag{6}$$

where m is the reduced mass and $A(k)$ is the distribution of momenta k in the initial packet $\chi(x|0)$.

Substituting eq 5 into eq 3 and inverting the Fourier transformation yields the 1-D version of eq 1

$$\chi(x|t) = \int_0^\infty F(E)\Phi(x|E)\mathrm{e}^{-iEt/\hbar}\,\mathrm{d}E \tag{7}$$

As mentioned in the Introduction, we propose applying this equation a number of times, using different energy filters $F(E)$. We will sometimes use the notation of Figure 1, such that $F(E)$ denotes the energy-distribution in the original wave packet $\chi(x|t)$ [used to generate $\Phi(x|\,E)$ via eqs 3 and 5] and $F_n(E)$ ($n = 1, 2, ...$) denotes the filters used in subsequent applications, each of which generates a different wave packet $\chi_n(x|t)$. Each $\chi_n(x|t)$ describes the time-evolution of an initial packet

$$\chi_n(x|0) = \int_0^\infty F_n(E)\mathrm{e}^{-ikx}\,\mathrm{d}E \tag{8}$$

A convenient general choice of the filters $F_n(E)$ is the form

$$F_n(E) = |F_n(E)|\mathrm{e}^{-ikx_0} \tag{9}$$

Strictly speaking, it is only the modulus $|F_n(E)|$ which acts as the "energy filter" and which can be used to generate packets $\chi_n(x|t)$ that describe the dynamics in different energy ranges. The phase e^{-ikx_0} determines the position of $\chi_n(x|0)$, which it localizes about $x = x_0$. The width of the packet about x_0 depends on the particular form of $|F_n(E)|$. For example, if we choose $|F_n(E)| = \exp(-k^2\sigma^2/2)$, then $\chi_n(x|0)$ is a Gaussian of width σ.

We emphasize that the packets $\chi_n(x|t)$ obtained by applying eq 7 are identical to those that would have been obtained by taking the initial packet $\chi_n(x|0)$ and propagating it using the time-evolution operator. Clearly, for a realistic (multidimensional) scattering problem, the computer time required to apply eq 7 is tiny in comparison with the time required to repeat the wave packet propagation. Hence, eq 7 is a practical way of exploiting the availability of large amounts of cheap disk space, to repeatedly generate a series of wave packets $\chi_n(x|t)$, corresponding to different initial packets. The only restrictions on the endless variety of different packets that may be recovered are the restrictions on the energies E and positions x at which $\Phi(x|E)$ is known. Hence, the filters $F_n(E)$ must be contained within $F(E)$, and $\chi_n(x|t)$ cannot be determined at those values of x that lie on the side of $\chi(x|0)$ away from the potential. Note that we have assumed in the above that $\Phi(x|E)$ is obtained from a wave packet propagation, via eqs 3 and 5. However, one could (at least in principle) generate $\Phi(x|E)$ on a grid of E using a time-independent (e.g., coupled-channel) method.

B. Plane Wave Packet (PWP) Method. To generalize the above to reactive and inelastic scattering, we introduce the plane

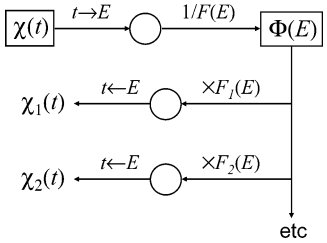

Figure 1. Schematic picture of the simple filtering ideas discussed in this paper. A wave packet propagation generates $\chi(t)$, which contains within it a superposition of energy-domain wave functions $\Phi(E)$ multiplied by an energy filter $F(E)$. A variety of wave packets $\chi_1(t)$, $\chi_2(t)$, etc. may then be generated from $\Phi(E)$, simply by extracting the $\Phi(E)$, then multiplying by a variety of new filters $F_1(E)$, $F_2(E)$, etc., and taking the Fourier transform.

wave packet (PWP) method, which obtains the differential cross sections (DCS) from wave packets showing how the products of a collision scatter into space. The PWP method has been described in several recent publications,[20−22] and a complete derivation of it will be published shortly.[28] Here, we give a brief summary of the method, as applied to A + BC reactive scattering.

The PWP method describes the scattering in terms of a time-dependent wave packet $\chi_{\lambda_0}(\mathbf{R}, r, \gamma, \alpha|t)$, which, at time $t = 0$, takes the form

$$\chi_{\lambda_0}(\mathbf{R}, r, \gamma, \alpha|0) = \chi_{\text{plane}}(R, \theta)\phi_{v_0}(r)Y_{j_0\Omega_{j_0}}(\gamma, \alpha) \quad (10)$$

The function $\chi_{\text{plane}}(R, \theta)$ is a plane wave packet

$$\chi_{\text{plane}}(R, \theta) = A(z - z_0)e^{i\bar{k}_0 z} \text{ with } z = R\cos\theta \quad (11)$$

which has an average momentum $\bar{k}_0$ along the z axis and is localized about $z = z_0$. The z axis is defined to be the initial approach direction of A + BC in center-of-mass (COM) scattering coordinates $\mathbf{R} = (R, \theta, \phi)$, such that $z = R\cos\theta$. The functions $\phi_{v_0}(r)$ and $Y_{j_0\Omega_{j_0}}(\gamma, \alpha)$ describe the initial vibrational and rotational states of BC, as a function of the internal stretch coordinate r and the rotation coordinates (γ, α). The index λ_0 refers to the set of quantum numbers $\{v_0, j_0, \Omega_{j_0}\}$.

As time evolves, $\chi_{\lambda_0}(\mathbf{R}, r, \gamma, \alpha|t)$ moves toward the scattering potential. When it reaches the strong-interaction region (where all three atoms are close together), the reagent coordinates $(\mathbf{R}, r, \gamma, \alpha)$ are switched to the product coordinates $(\mathbf{R}', r', \gamma', \alpha')$ (each primed coordinate being the AC + B counterpart to the A + BC unprimed coordinate). The ensuing scattering into space of $\chi_{\lambda_0}(\mathbf{R}', r', \gamma', \alpha'|t)$ is then related to the DCS as follows.

First, $\chi_{\lambda_0}(\mathbf{R}', r', \gamma', \alpha'|t)$ is projected onto a set of "probe" packets $\chi_\lambda(\mathbf{R}', r', \gamma', \alpha'|\theta'_p)$, each of which is a *fixed* plane wave packet that is perpendicular to the direction $\theta' = \theta'_p$. [Probe packets were first used in fixed-J scattering, where they were referred to as "test" functions.[29]] This yields the time-dependent scattering amplitude

$$f_{\lambda\leftarrow\lambda_0}(\theta'_p, t) = \langle\chi_\lambda(\theta'_p)\,|\chi_{\lambda_0}(t)\rangle \quad (12)$$

from which is obtained the time-dependent DCS

$$\frac{d\sigma_{\lambda\leftarrow\lambda_0}(\theta'_p, t)}{d\Omega} = |f_{\lambda\leftarrow\lambda_0}(\theta'_p, t)|^2 \quad (13)$$

The (experimentally measurable) energy-domain DCS is obtained by taking the Fourier transform of $f_{\lambda\leftarrow\lambda_0}(\theta', t)$ (having dropped the p subscript) to yield

$$g_{\lambda\leftarrow\lambda_0}(\theta', E) = \frac{1}{2\pi\hbar}\int_0^\infty e^{iEt/\hbar} f_{\lambda\leftarrow\lambda_0}(\theta', t)\,dt \quad (14)$$

The energy-domain scattering amplitude is then obtained from

$$f_{\lambda\leftarrow\lambda_0}(\theta', E) = \frac{\hbar^2 kk'}{4\pi^2 im\,A(k)A^*(k')}\,g_{\lambda\leftarrow\lambda_0}(\theta', E) \quad (15)$$

where $A(k)$ and $A(k')$ are the distributions of momenta k and k' contained in respectively the initial and probe plane wave packets, and m and m' are the A + BC and AC + B reduced masses. The DCS is then given by the standard formula

$$\frac{d\sigma_{\lambda\leftarrow\lambda_0}(\theta', E)}{d\Omega} = \frac{mk'}{m'k}|f_{\lambda\leftarrow\lambda_0}(\theta', E)|^2 \quad (16)$$

Hence, the energy-domain DCS is related, directly, via the time-dependent DCS and scattering amplitude, to the wave packets $\chi_{\lambda_0}(\mathbf{R}', r', \gamma', \alpha'|t)$, which visualize the scattering of the AC + B products into space. These wave packets may therefore be used to interpret the energy-domain DCS. Examples of such interpretations are given in refs 20−22.

C. Energy Filters in the PWP Method. We now explain how to enhance the interpretative power of the PWP method by incorporating the filtering ideas of section II.A.

First, the analogy to eq 7 in the PWP method is

$$\chi_{\lambda_0}(\mathbf{R}', r', \gamma', \alpha'|t) = \int_0^\infty F(E)\Phi_{\lambda_0}(\mathbf{R}', r', \gamma', \alpha'|E)e^{-iEt/\hbar}\,dE \quad (17)$$

where $\Phi_{\lambda_0}(\mathbf{R}', r', \gamma', \alpha'|E)$ is the time-independent wave function with plane wave boundary conditions.[30] Substituting this expression into eqs 12, 14, and 15 and specifying that the probe packets contain a flat distribution of energies (such that $A(k')/k' = 1$) yields

$$f_{\lambda\leftarrow\lambda_0}(\theta', t) = N\int_0^\infty F(E)f_{\lambda\leftarrow\lambda_0}(\theta', E)e^{-iEt/\hbar}\,dE \quad (18)$$

where the constant $N = 4\pi^2\hbar^2 i/m'$. Clearly, this equation may be substituted into eq 13 to yield the time-dependent DCS corresponding to the wave packet of eq 17. The corresponding energy-domain DCS is

$$\frac{d\sigma^{\text{filt}}_{\lambda\leftarrow\lambda_0}(\theta', E)}{d\Omega} = N^2|F(E)|^2\,\frac{d\sigma_{\lambda\leftarrow\lambda_0}(\theta', E)}{d\Omega} \quad (19)$$

Hence, one may use eq 19 to isolate a feature of interest in the DCS and then use eqs 17 and 18 in order to generate the wave packet and time-dependent DCS that visualize the dynamics responsible for the feature. This process may be repeated any number of times, so as to isolate different features and to experiment with different types of filter (to check, e.g., whether the filtering has introduced numerical artifacts into the time-dependent dynamics).

If this filtering technique is to be of practical use, however, it must also filter as a function of the scattering angle θ', because features in a DCS, caused by different reaction mechanisms, are likely to be found within a specific region of E and θ'. The simplest way to make this generalization is to introduce J-dependent filters $F_J(E)$, with J the total angular momentum quantum number.[31] Hence, we generalize eq 17 to

$$\chi_{\lambda_0}(\mathbf{R}, r, \gamma, \alpha|t) = \int_0^\infty \sum_{J=0}^{J_{max}} F_J(E)\phi_{\lambda_0 J}(\mathbf{R}', r', \gamma', \alpha'|E)\, e^{-iEt/\hbar}\, dE \quad (20)$$

where $\phi_{\lambda_0 J}(\mathbf{R}', r', \gamma', \alpha'|E)$ is the Jth partial wave of $\Phi_{\lambda_0}(\mathbf{R}', r', \gamma', \alpha'|E)$. The analogous expression for the time-dependent scattering amplitude is

$$f_{\lambda\leftarrow\lambda_0}(\theta', t) = N\int_0^\infty \frac{1}{2ik}\sum_{J=0}^{J_{max}}(2J+1)F_J(E)S^J_{\lambda_0\lambda}(E)d^J_{\Omega_0\Omega}(\theta')e^{-iEt/\hbar}\, dE \quad (21)$$

where $S^J_{\lambda_0\lambda}(E)$ is an element of the **S** matrix. Similarly, the filtered energy-domain DCS is given by

$$\frac{d\sigma^{filt}_{\lambda\leftarrow\lambda_0}(\theta', E)}{d\Omega} = N^2\left|\frac{1}{2ik}\sum_{J=0}^{J_{max}}(2J+1)F_J(E)S^J_{\lambda_0\lambda}(E)d^J_{\Omega_0\Omega}(\theta')\right|^2 \quad (22)$$

To apply these equations, one proceeds as follows. First, one chooses the energy filters $F_J(E)$ such that the filtered DCS reproduces (and isolates) a feature in the (unfiltered) DCS that one wants to interpret. To achieve this, the $F_J(E)$ could be chosen, either by experimenting with eq 22 [choosing different $F_J(E)$ until $d\sigma^{filt}_{\lambda\leftarrow\lambda_0}(\theta', E)/d\Omega$ reproduces the desired feature sufficiently accurately] or by first decomposing the feature into its partial wave components, then determining the $F_J(E)$ using the fixed-J reaction probabilities. The latter approach is demonstrated in section III.B below. Having determined the $F_J(E)$, the time-dependent wave packet and scattering amplitude are generated using eqs 20 and 21. We emphasize that, despite the appearance of the **S** matrix elements in eqs 21 and 22, the direct relation which the PWP method affords between the spatially evolving wave packet and the DCS is still present, except that it now exists between the wave packet and the *filtered* DCS $d\sigma^{filt}_{\lambda\leftarrow\lambda_0}(\theta', E)/d\Omega$.

D. Focused Plane Wave Packets. In addition to filtering out specific features in the DCS, the $F_J(E)$ also determine the position of the initial plane wave packet $\chi_{plane}(R, \theta)$ and of the probe wave packets $\chi_\lambda(\mathbf{R}', r', \gamma', \alpha'|\theta'_p)$. By analogy with eq 9, a useful general form of $F_J(E)$ is

$$F_J(E) = |F_J(E)|e^{-ikz_0 + ik'R'_p} \quad (23)$$

which localizes the initial plane wave packet around $z = z_0$ and distributes the probe packets around a semicircle of radius R'_p. Successive applications of eq 20 can use different values of z_0 and R'_p and thereby experiment with the effect on $\chi_{\lambda_0}(\mathbf{R}, r, \gamma, \alpha|t)$ of varying the position of the initial and probe packets. This allows one to investigate the effects of spreading on the wave packet. In particular, in many systems, it will allow one to minimize the spreading by using *focused* plane wave packets.

Focused wave packets were introduced into (fixed-J) reactive scattering by Gögtas et al.[32] and later used by Monnerville and co-workers,[33] in order to make the wave packet compact in the strong-interaction region. It is straightforward to apply such focusing to plane wave packets. Figure 2 compares an unfocused plane wave packet with a focused plane wave packet. The focused packet reverses the spreading suffered by the unfocused packet, starting off broad (but confined to $z < -12$ bohr) and then becoming narrow and "focused" by the time it has reached $z = -3$ bohr.

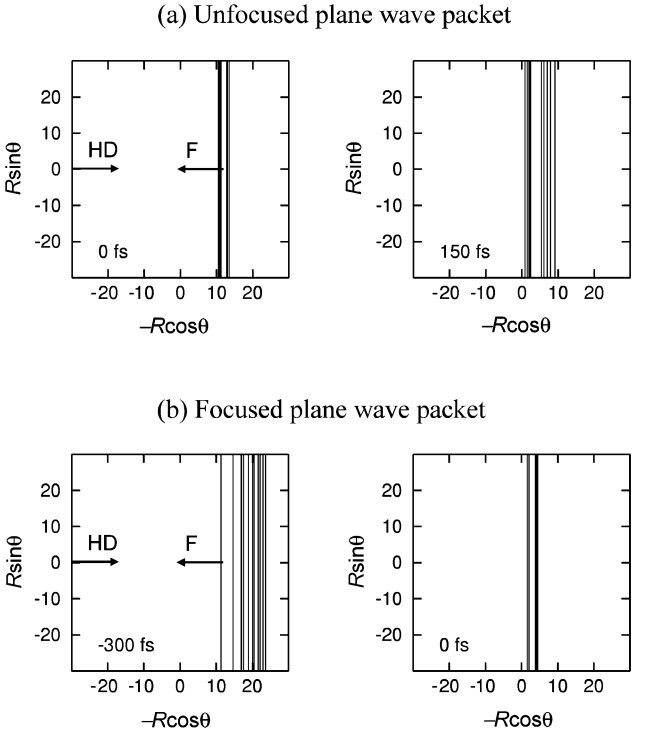

Figure 2. Illustration of the (a) unfocused and (b) focused plane wave packets used to generate the results for F + HD, shown in Figures 3−7. The coordinates R and θ are the F + HD scattering coordinates, defined in section II.B.

Such focusing is achieved by setting z_0 to a small value of z, where the scattering potential *cannot* be neglected. The initial packet (which is localized about z_0) is then propagated anti-causally, in the absence of the scattering potential, until such a time, $t = -T$, that it has moved sufficiently far out that the scattering potential can be neglected. This (broad) packet is then defined to be the initial wave packet, so that the propagation starts at $t = -T$.[34] In the absence of the scattering potential, therefore, the initial wave packet at $t = -T$ will have become focused about $z = z_0$ at $t = 0$. Figure 2b was obtained by localizing the packet about $z_0 = -3$ bohr and then propagating it anti-causally until $t = -300$ fs, by which time it was confined to $z < -12$ bohr. Propagating this packet from $t = -300$ fs then produces a packet which is focused about $z = -3$ bohr at $t = 0$ fs.

The anticausal propagation must be done under free-wave conditions, otherwise the scattering potential will produce a superposition of different channels in the initial packet at $t = -T$. Hence, there is no guarantee that, in the full calculation, with the scattering potential included, the initial packet at $t = -T$ will have become focused at $z = z_0$ at $t = 0$. However, previous work[32,33] has shown that the focusing works well for a variety of reactions, when z_0 is chosen to be in the strong-interaction region.

There is no need to evaluate the anticausal propagation explicitly, when applying the filters of eq 23. In fact, one does not even have to work out T. It is enough to know that, by a sufficiently negative $t = -T$, the packet will have reached a region that is far enough out that the scattering potential can be neglected. One then applies eq 20 using a value of z_0 in eq 23 that is in the strong-interaction region. The resulting $\chi_{\lambda_0}(\mathbf{R}, r, \gamma, \alpha|t)$ is then focused at z_0 at $t = 0$ (in the sense just defined). [To prove this, one has only to note that the energy composition of the wave packet at time $t = -T$ is identical to the composition

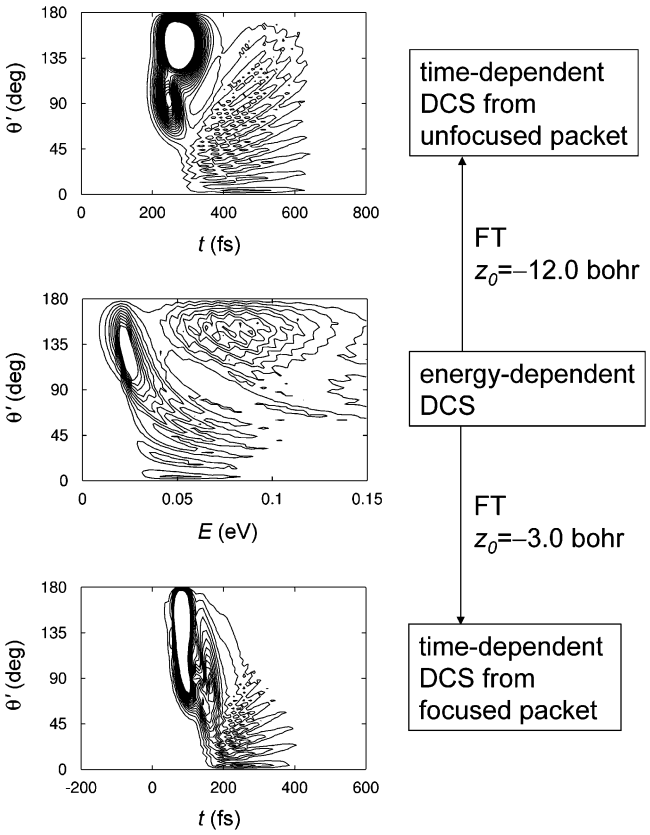

Figure 3. Time- and energy-dependent differential cross sections (DCS) for F + HD($v_0 = 0$, $j_0 = 0$) → HF ($v = 2$, $j = 0$) + D. The "ridge" feature is clearly visible in the energy-dependent DCS, sweeping round from $\theta' = 180°$ at threshold, to $\theta' = 0°$ at $E = 0.05$ eV. The time-dependent DCSs are obtained from the energy-domain scattering amplitudes, using filters $F_J(E)$ corresponding to the unfocused and focused plane wave packets of Figure 2.

at time $t = 0$.] We demonstrate the use of eq 20 to generate focused plane wave packets in section III.B below.

III. Demonstration on the F + HD Reaction

We now demonstrate the use of the filter techniques introduced in section II, by interpreting the DCS for the reaction F + HD($v_0 = 0$, $j_0 = 0$) → HF($v = 2$, $j = 0$) + D, in the collision energy range $E = 0-0.15$ eV. This is a good example, because, as shown in Figure 3, the energy-dependent DCS has a distinct "ridge" feature, going from $\theta' = 180°$ near threshold, to $\theta' = 0$ near $E = 0.075$ eV. This feature is known from previous work, most notably refs 19, 25, and 26, to be caused by a superposition of Feshbach resonances. Our aim here is to use the filters to isolate the "ridge" feature from the rest of the DCS, in order to produce wave packets visualizing the formation and decay of the FHD complex.

The energy-domain DCS of Figure 3, the **S** matrix elements $S^J_{\lambda_0\lambda}(E)$, and the partial wave functions $\phi_{\lambda_0 J}(\mathbf{R}', r', \gamma', \alpha'|E)$ were obtained from wave packet calculations on the Stark−Werner surface.[35] These calculations employed the recent RPD (reactant−product decoupling[36−39]) method of the author;[39] full details are given in ref 22. It suffices here to point out that these calculations serve as the initial "$\chi(t) \rightarrow \Phi(E)$" step, represented schematically in Figure 1. That is, they are used to generate $S^J_{\lambda_0\lambda}(E)$ and $\phi_{\lambda_0 J}(\mathbf{R}', r', \gamma', \alpha'|E)$ on a grid of energies (with grid spacing 2.5 meV), for all values of J ($0 \rightarrow 30$) necessary to generate various plane wave packets and time-dependent DCS, using different choices of $F_J(E)$ in eqs 20 and 21.

A. Focused and Unfocused Wave Packets. The time-dependent DCSs in Figure 3 were generated by applying eq 21, using filters $F_J(E)$ chosen to be independent of J and flat over the entire 0.15 eV energy range of the energy-domain DCS. The $F_J(E)$'s die off rapidly and smoothly to zero at $E = 0$ and 0.15 eV. This is achieved by choosing each $|F_J(E)|$ to be the Fourier transform of a distributed approximating functional (DAF), which is a type of wavelet, defined in ref 40. The $F_J(E)$ take the form

$$|F_J(E)| = \frac{1}{\sqrt{2\pi}} e^{-\bar{E}^2} \sum_{m=0}^{M/2} \frac{1}{m!} \bar{E}^{2m} \text{ where } \bar{E}^2 = \frac{1}{2}(E - E_J)^2\sigma^2 \quad (24)$$

The parameters were set to $M = 88$, $\sigma = 40$ eV^{-1}, and $E_J = 0.17$ eV. Hence, the time-dependent DCS of Figure 3 are obtained with no filtering at all in θ', and they give an unbiased picture of all of the dynamics that produce the energy-domain DCS across the entire 0.15 eV energy range shown.

The time-dependent DCSs of Figure 3 were obtained with $z_0 = -12$ bohr (unfocused) and $z_0 = -3$ bohr (focused). In both cases, the probe packets were fixed at $R'_p = 12$ bohr. The time evolution of the unfocused and focused plane wave packets, in the absence of the FHD scattering potential, is shown in Figure 2. The time evolution produced with the scattering potential (so that the packets undergo the F + HD reaction) is shown in Figure 4.[41] The scattered packets are projected onto the ($v = 2$, $j = 0$) and ($v = 3$, $j = 0$) quantum states of HF, so that the pink [($v = 2$, $j = 0$)] packets in Figure 4, parts a and b map onto respectively the unfocused and focused time-dependent DCS of Figure 3.

As already mentioned, the fact that the free-wave packets of Figure 2b focus at $z_0 = -3$ bohr, at $t = 0$, is no guarantee that the packets in the full calculations should be similarly focused. However, it is evident from Figures 3 and 4 that the focusing at $z_0 = -3$ bohr has worked well and produced packets and time-dependent DCS that are much more compact than their unfocused counterparts.

The focused DCS and wave packets give new insight into the timing of the "ridge" mechanism with respect to the other, mainly direct, mechanisms. In the unfocused DCS, the ridge mechanism appears as a very broad feature, which lags behind the two direct mechanisms by about 250 fs. In the focused DCS, however, the "ridge" mechanism is much closer to the direct mechanisms, appearing first in the backward direction, where it overlaps the direct mechanisms. Hence, much of the time-delay that appears in the unfocused DCS between the ridge and direct mechanisms is an artifact, brought about by the spreading of the wave packet in the entrance channel. Evidently, another such artifact (in the unfocused DCS) is that the ridge mechanism appears first in the sideways direction, at about $\theta' = 45°$, rather than the backward direction. Thus, the unfocused wave packet of Figure 4a gives a picture of the decay of the FHD complex which contains some artifacts, and these artifacts are removed when packet is focused in Figure 4b.

B. Isolating and Focusing the "Ridge" Mechanism. Although Figure 4b has removed the artifacts present in Figure 4a, it is not very useful in illustrating the ridge mechanism. This is because, in removing the artificial contributions to the time delay, the focusing has conflated the early part of the ridge mechanism with the direct mechanism. However, the energy-domain DCS (Figure 3) shows that the ridge mechanism may readily be isolated, because it scatters the products into a different region of θ' and E from the direct mechanism. We

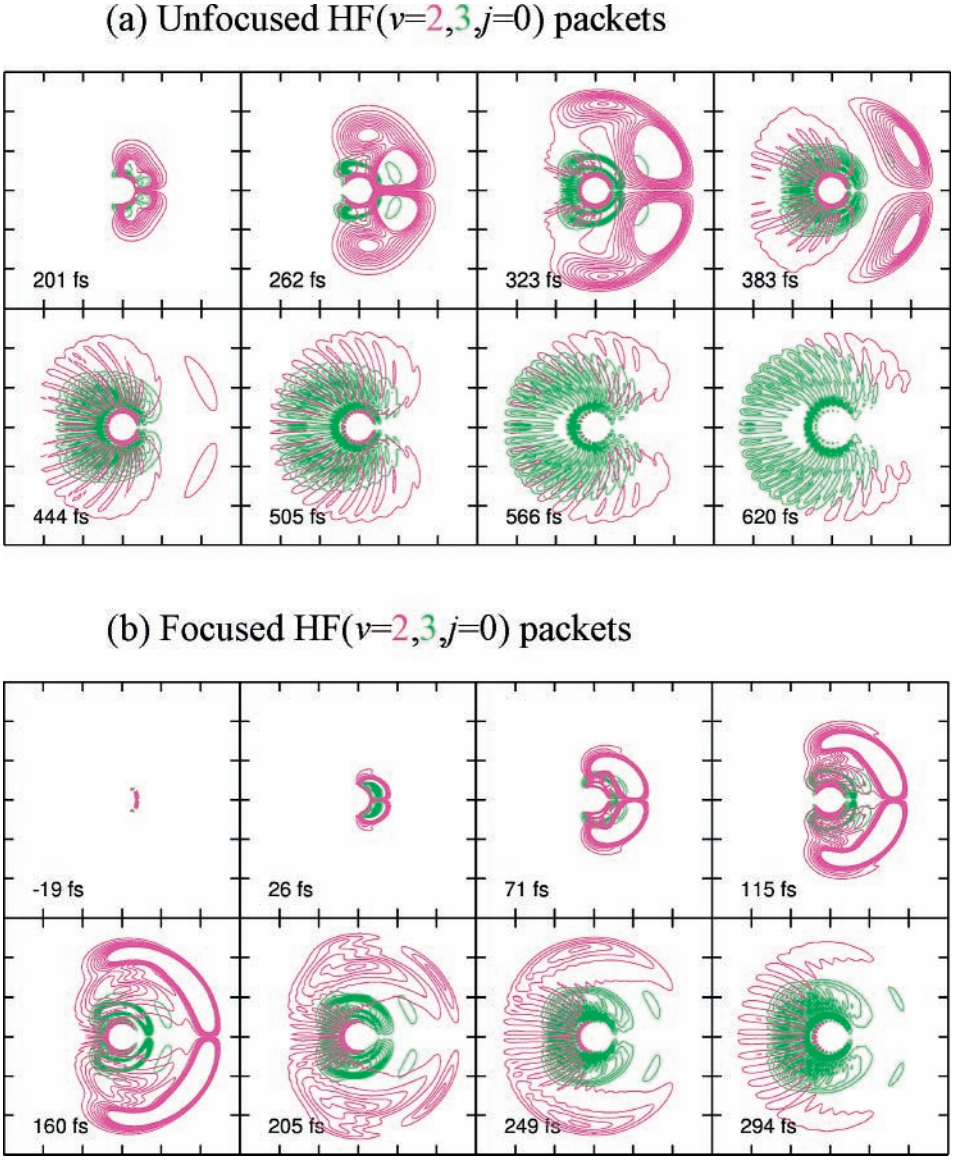

Figure 4. Snapshots from plane wave packet movies of the F + HD($v_0 = 0$, $j_0 = 0$) reaction, obtained using the same filters that generated the (a) unfocused and (b) focused time-dependent DCS of Figure 3. The wave packets have been projected onto the ($v = 2$, $j = 0$) and ($v = 3$, $j = 0$) quantum states of HF. The dimensions of each frame are the same as in Figure 2. The complete wave packet movies may be viewed on the web (http://www.ex.ac.uk/~scalthor/movies.htm).

may therefore use J-dependent filters $F_J(E)$, as described in section II.D, to isolate this region of θ' and E.

To this end, we use filters $|F_J(E)|$ of the form of eq 24, which are made to depend on J through the parameter E_J. The latter is chosen such that, for each partial wave, the filter $|F_J(E)|$ encloses the resonance peak that contributes to the ridge mechanism. The other parameters took the values $M = 440$ and $\sigma = 100$ eV^{-1}. The effects of $|F_J(E)|$ on selected partial waves are illustrated in Figure 5, which shows fixed-J reaction probabilities obtained with, and without, multiplication by the $|F_J(E)|$. The values of E_J are listed in Table 1. They were determined by eye; a more sophisticated treatment could derive the filters by fitting the resonance peaks to a Breit-Wigner line shape.[30] The simple treatment used here is likely to capture most of the dynamics responsible for the ridge mechanism, though we must expect small artifacts, where the $|F_J(E)|$ have "chopped off" the resonance peaks where they merge into the direct scattering feature.

Superposing the filtered partial waves according to eq 22 gives the energy-domain DCS $d\sigma^{\text{filt}}_{\lambda\leftarrow\lambda_0}(\theta', E)/d\Omega$ shown in Figure 6. Clearly, the J-dependent filters $|F_J(E)|$ have successfully isolated the ridge feature from the rest of the DCS, meaning that the $F_J(E)$ can be used in eqs 21 and 20, to generate the time-dependent DCS and wave packets that visualize the dynamics of the ridge mechanism. The time-dependent DCS are shown in Figure 6. They were obtained from focused and unfocused initial wave packets, using the same z_0 and R'_p as in section III.A. The corresponding scattering wave packets are shown in Figure 7, projected onto the ($v = 2$, $j = 0$) and ($v = 3$, $j = 0$) quantum states of HF. The initial packets may be thought of as the focused and unfocused plane waves of Figure 2, except that only those components of the packet about to undergo the ridge mechanism are permitted to react.

By comparing the unfocused DCS and wave packet of Figures 3 and 4 with Figures 6 and 7, we see that the filtering has isolated the time-delayed ridge mechanism, though it has introduced some differences. In the unfocused DCS, the isolated ridge mechanism of Figure 6 looks flatter than the nonisolated ridge mechanism of Figure 3, in the backward region where the latter borders on the direct mechanism. This difference shows

TABLE 1: Values Taken by the Parameter E_J of Equation 24, Used to Isolate the F + HD Ridge Mechanism and Produce the Results in Figures 5−7

J	0−4	5	6	7,8	9	10	11	12	13	14
E_J/eV	0.065	0.070	0.076	0.080	0.085	0.090	0.095	0.100	0.105	0.110
J	15,16	17	18	19	20	21	22	23	24	25−30
E_J/eV	0.120	0.130	0.140	0.145	0.150	0.158	0.167	0.175	0.185	0.195

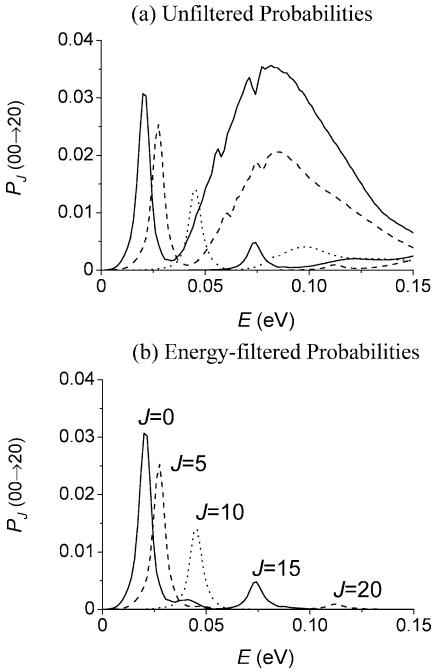

Figure 5. Selected fixed-J reaction probabilities $P_J(00 \rightarrow 20)$ for F + HD($v_0 = 0$, $j_0 = 0$) → HF ($v = 2$, $j = 0$) + D. The $P_J(00 \rightarrow 20)$ in panel a are unfiltered; the $P_J(00 \rightarrow 20)$ in panel b have been multiplied by the filters $F_J(E)$, of Table 1, to isolate the Feshbach resonance peaks. Each line in panel a corresponds to the same value of J as the corresponding line in panel b.

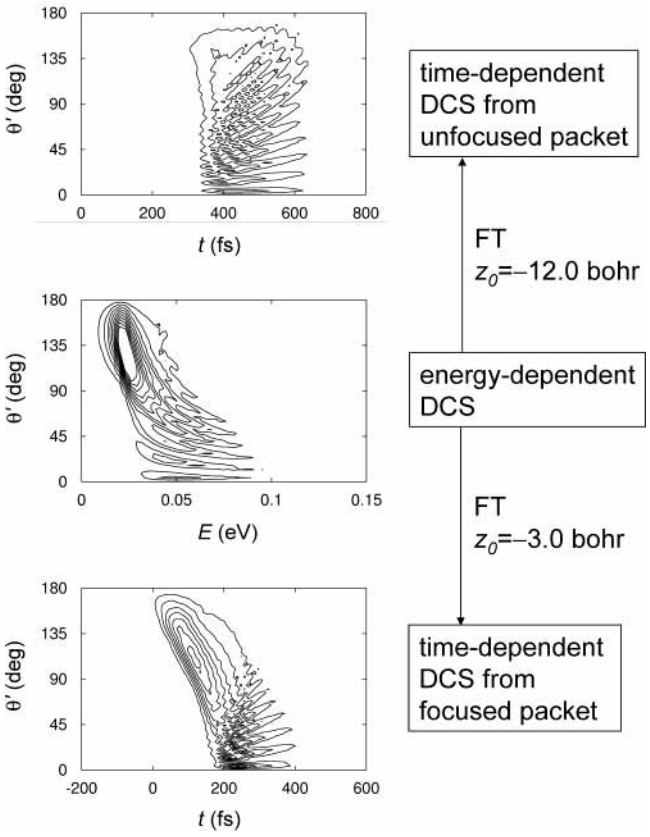

Figure 6. As Figure 3, except that the filters $F_J(E)$ illustrated in Figure 5 have been applied. Thus, the energy-domain DCS contains only the superposition of Feshbach resonances that produces the ridge. The time-dependent DCSs show the time-evolution of the ridge, obtained using unfocused and focused plane wave packets.

up in the unfocused wave packets [Figures 4a and 7a] in the 323 and 383 fs snapshots, when the HF from the ridge mechanism is starting to emerge from the FHD trapped in the inner ring. These differences could be artifacts (introduced as mentioned above), or they could be caused by interference between the ridge mechanism and the tail-end of the direct mechanism. Despite these differences, it is clear that the filters $|F_J(E)|$ have separated out the bulk of the ridge mechanism from the other mechanisms.

The advantage of isolating the ridge mechanism is that we can focus it without conflating it with the other mechanisms (as happened in Figures 3 and 4). In the unfocused packets of Figures 4a and 7a, the ridge mechanism emerges first in the sideways direction, then in the forward direction, and then it shifts round into the backward direction. This behavior is evidently an artifact of the spreading of the packet, because it disappears completely in the focused packet of Figure 7b. In the latter, the FHD complex is formed first in the backward direction, and then it rotates round into the forward direction. The complex throws out HF($v = 2$) product as it rotates, and it has completely decayed after about half a revolution. There is evidence of interference in the forward direction. Most likely this is a Glory effect, caused by the packet rotating by somewhat more than 180°, so that the nearside and farside parts interfere.[42] Note that, during the first 90° of rotation, the FHD complex is being continuously added to, as successively higher impact parameters reach the scattering potential. The rotating FHD remains quite compact, despite being a superposition of Feshbach resonances, each with a different angular momentum quantum number J. Evidently, the complex does not live long enough to spread much around the θ' coordinate.

Hence, the filters $|F_J(E)|$ have successfully isolated the low energy ridge from the DCS. They have produced a focused wave packet that shows that the ridge is caused by the FHD complex rotating and decaying like a "Catherine wheel".[43] As mentioned above, the ridge has been measured experimentally, and shown to be a superposition of Feshbach resonances.[19,25,26] The Stark-Werner potential energy surface[35] used here is known to have deficiencies in the exit channel, but the DCS obtained from it is in good overall agreement with experiment up to about $E =$ 0.05 eV.[19,25,26] Thus, we can be reasonably confident that the simple "Catherine wheel" picture of the ridge mechanism, given by Figure 7b is physically correct.

IV. Conclusions

The results of section III suggest that the filtering techniques introduced here are useful, general tools for interpreting reaction dynamics. Using different filters, it is straightforward to generate wave packets corresponding to different reaction mechanisms and to focus these packets. When combined with the plane wave packet (PWP) method, the filters allow one to produce focused wave packets, which visualize the dynamics of different features in the energy-domain DCS. Similar filtering should also prove

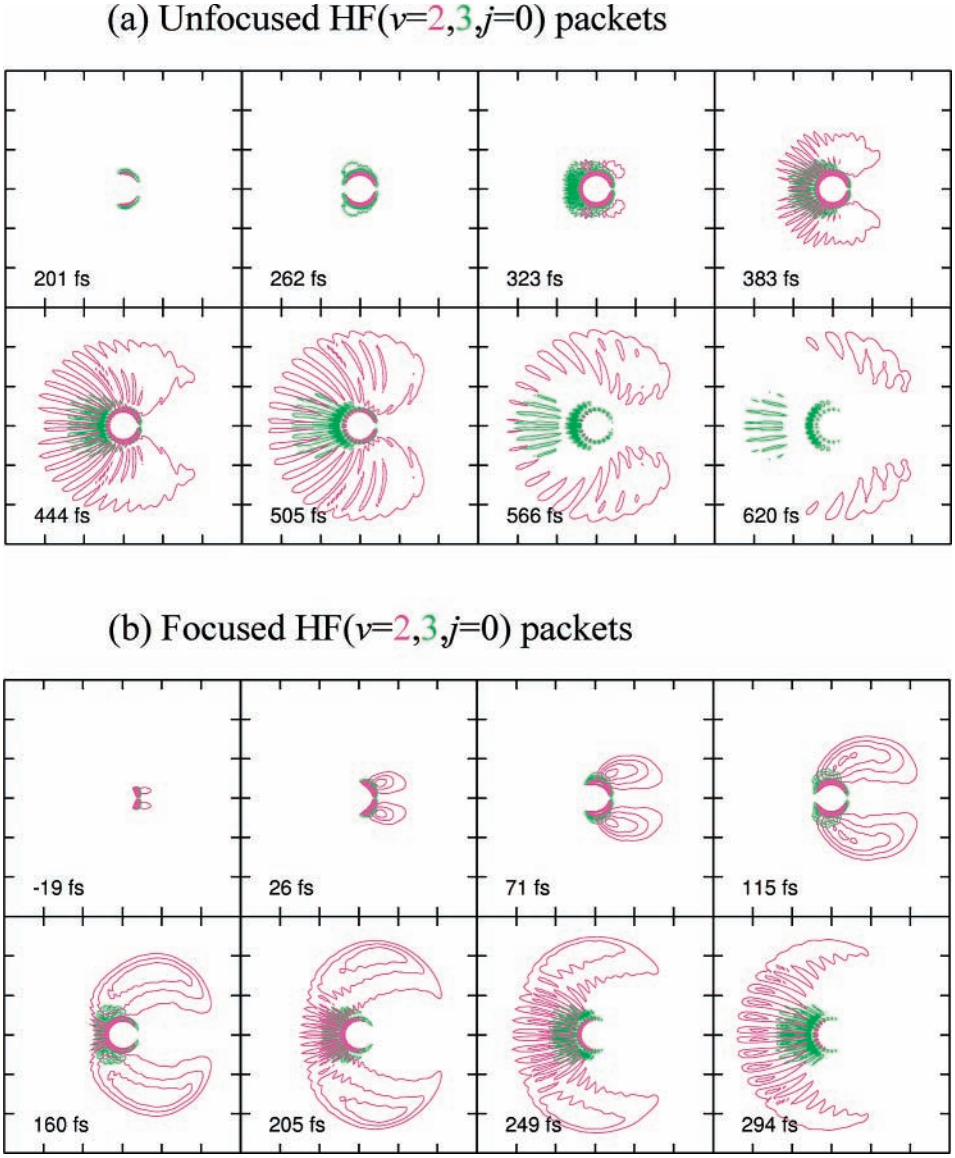

Figure 7. As Figure 4, except that the wave packets now correspond to the time-dependent DCS of Figure 6, and therefore show the time-evolution of the ridge mechanism only. Note the simple "Catherine wheel" behavior of the focused packet, which corresponds to the rotation and decay of the FHD complex. The complete wave packet movies may be viewed on the web (http://www.ex.ac.uk/~scalthor/movies.htm).

very useful when applied in fixed-J calculations. Moreover, the filtering can be applied in time-independent calculations, provided the wave function, or scattering amplitude, is obtained over a grid of energies.

There is considerable potential for extending the simple filtering ideas presented here. The evaluation of eq 1 [or its PWP generalizations in section II.C] is computationally trivial, in comparison with a wave packet propagation, and hence, it will be possible to develop algorithms which optimize the filters $F(E)$. Such algorithms could be based upon least-squares fitting, a variational principle, or a control procedure. Optimization criteria could aim to yield, for example, the most focused wave packet, the cleanest extraction of an individual mechanism, or the maximal separation in time between two mechanisms. Of course, all wave packets that contain the same spread of energies give physically equivalent descriptions of the reaction dynamics. However, some wave packets obscure the dynamics, for example by spreading, whereas others visualize it clearly. We have shown in this paper how the simple filtering ideas, embodied in eq 1, may be used to produce the latter type of wave packet.

The results obtained in section III for F + HD add to what was known previously about the mechanism that causes the low-energy ridge in the DCS. Previous work[19,25,26] had shown that the ridge is caused by a superposition of Feshbach resonances, produced by tunneling through the transition state. Recent work by the author[22] had obtained the first (nonfocused) PWP packets that showed the trapping and decay of the resulting FHD complex. By isolating and focusing the ridge mechanism, in section III, we have shown that the FHD produces the ridge by rotating through half a revolution, like a Catherine wheel. This explanation ties in nicely with previous work by Miller and Zhang,[44] who predicted, using semiclassical arguments, that such broad resonances would superpose to produce interesting ridge-like features in the differential cross section. We emphasize that the simple "Catherine wheel" picture is the result of rigorous quantum calculations and would have been very difficult to obtain without the filtering techniques introduced here.

Acknowledgment. It is a pleasure to acknowledge the continuing encouragement of Don Kouri, under whose inspired guidance I first entered the fascinating world of quantum wave packet dynamics. I thank the Royal Society for the award of a University Research Fellowship.

References and Notes

(1) *Femtochemistry and Femtobiology: Ultrafast Dynamics in Molecular Science*; Douhal, A., Santamaria, J., Eds.; World Scientific: Singapore, 2002.

(2) Weiss, J.; Hauschildt, J.; Schinke, R.; Haan, O.; Skokov, S.; Bowman, J. M.; Mandelshtam, V. A.; Peterson, K. A. *J. Chem. Phys.* **2001**, *115*, 8880.

(3) Balint-Kurti, G. G.; Orr-Ewing, A. J.; Beswick, J. A.; Brown, A.; Vasyutinskii, O. S. *J. Chem. Phys.* **2002**, *116*, 10760.

(4) van Harrevelt, R.; van Hemert, M. C. *J. Chem. Phys.* **2000**, *112*, 5777.

(5) Roncero, O.; Campos-Martínez, J.; Hernández, M. I.; Delgado-Barrio, G.; Villarreal, P.; Rubayo-Soneira, J. *J. Chem. Phys.* **2001**, *115*, 2566.

(6) Mowrey, R. C.; Kouri, D. J. *J. Chem. Phys.* **1986**, *84*, 6466.

(7) Kingma, S. M.; Somers, M. F.; Pijper, E.; Kroes, G.-J.; Olsen, R. A.; Baerends, E.-J. *J. Chem. Phys.* **2003**, *118*, 4190.

(8) Corriol, C.; Darling, G. R.; Holloway, S.; Andrianov, I.; Klamroth, T.; Saalfrank, P. *J. Chem. Phys.* **2002**, *117*, 4489.

(9) Huarte-Larrañaga, F.; Manthe, U. *J. Chem. Phys.* **2002**, *117*, 4635.

(10) Althorpe, S. C.; Clary, D. C. *Annu. Rev. Phys. Chem.* **2003**, *54*, 493.

(11) Sun, Y.; Mowrey, R. C.; Kouri, D. J. *J. Chem. Phys.* **1987**, *87*, 339.

(12) Neuhauser, D.; Baer, M. *J. Chem. Phys.* **1989**, *91*, 4651. Judson, R. S.; Kouri, D. J.; Neuhauser, D.; Baer, M. *Phys. Rev. A* **1990**, *42*, 351.

(13) Neuhauser, D.; Baer, M.; Judson, R. S.; Kouri, D. J. *Comput. Phys. Commun.* **1991**, *63*, 460.

(14) Zhang, D. H.; Light, J. C. *J. Chem. Phys.* **1996**, *104*, 4544.

(15) Zhu, W.; Dai, J. Q.; Zhang, J. Z. H.; Zhang, D. H. *J. Chem. Phys.* **1996**, *105*, 4881.

(16) Maiti, B.; Mahapatra, S.; Sathyamurthy, N. *J. Chem. Phys.* **2000**, *113*, 59.

(17) Balint-Kurti, G. G.; Gonzalez, A. I.; Goldfield, E. M.; Gray, S. K. *Faraday Discuss.* **1998**, *110*, 169.

(18) Russell, C. L.; Manolopoulos, D. E. *Chem. Phys. Lett.* **1996**, *256*, 465.

(19) Skodje, R. T.; Skouteris, D.; Manolopoulos, D. E.; Lee, S.-H.; Dong, F.; Liu, K. *J. Chem. Phys.* **2000**, *112*, 4536.

(20) Althorpe, S. C. *J. Chem. Phys.* **2002**, *117*, 4623.

(21) Althorpe, S. C.; Fernández-Alonso, F.; Bean, B. D.; Ayers, J. D.; Pomerantz, A. E.; Zare, R. N.; Wrede, E. *Nature* **2002**, *416*, 67.

(22) Althorpe, S. C. *Chem. Phys. Lett.* **2003**, *370*, 443.

(23) Aoiz, F. J.; Bañares, L.; Herrero, V. J.; Sáez Rábanos, V.; Stark, K.; Werner, H.-J. *J. Chem. Phys.* **1995**, *102*, 9248.

(24) See, for example: *Quantum Mechanics of Molecular Rate Processes*; Levine, R. D.; Oxford University Press: New York, 1969; p 129.

(25) Skodje, R. T.; Skouteris, D.; Manolopoulos, D. E.; Lee, S.-H.; Dong, F.; Liu, K. *Phys. Rev. Lett.* **2000**, *85*, 1206.

(26) Liu, K.; Skodje, R. T.; Manolopoulos, D. E. *Phys. Chem. Commun.* **2002**, *5*, 27.

(27) Kouri, D. J.; Hoffman, D. K. *Few-Body Syst.* **1995**, *18*, 203.

(28) Althorpe, S. C. *J. Chem. Phys.* submitted.

(29) Kouri, D. J.; Huang, Y.; Zhu, W.; Hoffman, D. K. *J. Chem. Phys.* **1994**, *100*, 3662.

(30) *Scattering Theory*; Taylor, J. R.; Krieger: Malabar, FL, 1983.

(31) Simply introducing a filter $F(E,\theta')$ will permit only the time-dependent amplitude $f_{\lambda\leftarrow\lambda_0}(\theta', t)$ to be generated, because a wave packet that scatters into the range of θ' contained in $F(E,\theta')$ will almost certainly have evolved through values of θ' outside this range before scattering.

(32) Gögtas, F.; Balint-Kurti, G. G.; Offer, A. R. *J. Chem. Phys.* **1996**, *104*, 7927.

(33) Monnerville, M. personal communication.

(34) This requires the lower limit in the integrals over t in section II to be changed from $t = 0$ to $t = -T$. Alternatively, one could shift time by $-T$, start the propagation off at $t = 0$, and introduce a phase of $\exp(iET/\hbar)$ into $\Phi(E)$.

(35) Stark, K.; Werner, H.-J. *J. Chem. Phys.* **1996**, *104*, 6515.

(36) Peng, T.; Zhang, J. Z. H. *J. Chem. Phys.* **1996**, *105*, 6072.

(37) Kouri, D. J.; Hoffman, D. K.; Peng, T.; Zhang, J. Z. H. *Chem. Phys. Lett.* **1996**, *262*, 519.

(38) Althorpe, S. C.; Kouri, D. J.; Hoffman, D. K. *J. Chem. Phys.* **1997**, *107*, 7816.

(39) Althorpe, S. C. *J. Chem. Phys.* **2001**, *114*, 1601.

(40) Huang, Y.; Zhu, W.; Kouri, D. J.; Hoffman, D. K. *J. Phys. Chem.* **1994**, *98*, 1868.

(41) The unfocused DCS and wave packet snapshots of Figures 3 and 4 were reported previously, in ref 22. They are replotted here for comparison with the other results, presented for the first time in section III.

(42) Dobbyn, A. J.; McCabe, P.; Connor, J. N. L.; Castillo, J. F. *Phys. Chem. Chem. Phys.* **1999**, *1*, 1115.

(43) A firework that forms a rotating wheel of colored flames. *American Heritage Dictionary of the English Language*, 4th ed.; Houghton Mifflin Co.: Boston, MA, 2000.

(44) Miller, W. H.; Zhang, J. Z. H. *J. Phys. Chem.* **1991**, *95*, 12.